PCCP

Cite this: *Phys. Chem. Chem. Phys.*, 2011, **13**, 7149–7153

www.rsc.org/pccp

PAPER

Why aggregated carbon nanotubes exhibit low quantum efficiency

Yu-Hsien Lin, Yao-Cheng Lai, Ching-Tung Hsu, Chia-Jung Hu and Wen-Kuang Hsu*

Received 29th November 2010, Accepted 18th February 2011
DOI: 10.1039/c0cp02691c

Aggregation of carbon nanotubes reduces quantum efficiency and the phenomenon is found to be related to photocurrent leakage through oxygenated lattices acting as low barrier intertube channels. This outcome is supported by calculation and optical excitation experiments.

Introduction

Owing to their low dimensionality, carbon nanotubes (CNTs) exhibit quantum confinement, and Coulomb force controlled inter-band transitions have been verified by field modulated conductivity and photoexcitation experiments.[1] For an ideal CNT with electronic symmetry, the occupation probability of excitons is essentially limited by dipole forbidden states, and optical resonance mainly originates from the van-Hove singularities associated two-electron band structure.[2] In practice, the radiative lifetime (W_r) involves defects induced multi-transitions, and optically allowed states are mostly populated at low energy regimes.[3] For example, the W_r is found to be two orders of magnitude greater than that of conventional molecular systems, and enhanced fluorescence emission emerges at < 100 K.[4,5] The quantum efficiency (η), however, decreases as CNTs aggregate, and nonradiative relaxation is believed to occur through phonon dissipation at tube–tube contacts.[6] In fact, the energy barrier (E_a) for intertube hopping is much greater than that of the on-tube mechanism, and a study gives E_a = 150–250 meV for the former and 1–4 meV for the latter.[7,8] Accordingly, the low η must originate from a mechanism that has not been discussed. In this work, bundles of single-walled CNTs (SWCNTs) are characterized by four-probe measurements, and low E_a is found to be related to oxygenation created localized states near to the Fermi level (E_F). Upon photoexcitation, the optically-created carriers tend to hop transversely through oxygenated groups acting as low barrier intertube channels, and this effect accounts for the low η.

Experimental

SWCNTs made by ferrocene pyrolysis are heated in air (400 °C, 30 min) to remove surface carbonaceous impurities, and encapsulated catalytic particles are removed by dispersing oxidized materials in diluted nitric acid at room temperature (RT, 2 h). It is worth mentioning that SWCNT purification usually employs hot nitric acid as an oxidant, and ester and carboxyl groups created at opened edges (cut tubes) have been verified by blue-shifted infrared spectra (IR).[9,10] The acid treatment at RT, however, evades tube cutting, as is supported by FT-IR (Bomem, DA8.3, 0.5 cm^{-1} resolution, 1 μm nanotube film by 75° grazing incident angle reflectance technique) and Raman (Horiba HR800, 632.8 nm excitation, He–Ne laser beam) data in the following text. Purified SWCNTs are deposited onto Al-electrode coated silicon substrate, and the electrical connections are made into a bundle consisting of 10–15 SWCNTs with lengths of 1.7 ± 0.1 μm, as revealed by a scanning electron microscope (SEM, JEOL JSE-6500F, field emission at 25 keV) (Fig. 1a). The device is then placed in a vacuum chamber (1×10^{-5} torr) equipped with a Cermax xenon optic fiber, and the nanotubes are spotted by a spectral monochromator laser (5 ± 1 μm, 658 nm, Power Technology-LDCU12/7891) (Figs 1a and b). The photoexcitation is evident from the sudden decrease in device resistance, and the photocurrent generation is recorded *in situ* by a Keithley-2400 power supply with background noise controlled at ±0.5 nA. In our study, the built-in-potential is small at the tube–lead contacts, and four-probe measurements reveal 0.01 eV at zero bias voltage, attributable to the similar work function between Al and the SWCNTs (4.25–4.28 eV). In other works, the photocurrent is mostly created by optically excited SWCNTs, and the contribution from the Schottky-like diodes at the source and drain electrodes is negligible.

Results and discussion

Fig. 1c plots device resistance *vs.* temperature at beam-on (lower) and -off states (upper), and a negative temperature coefficient of resistivity ($d\rho/dT$) is detected at 60–300 K. Compared with dark conditions, the resistance of the optically excited bundle is lower by 2.5% at RT, by 22% at 150 K, and by 46% at 60 K; the corresponding $d\rho/dT$ being -2.5×10^{-3} K^{-1} at RT and -9.6×10^{-4} K^{-1} at 60 K. Below 60 K, a metallic phase emerges and $d\rho/dT$ appears to be 3×10^{-3} K^{-1} and 8.7×10^{-4} K^{-1} for dark and bright conditions respectively.

Department of Materials Science and Engineering, National Tsing Hua University, HsinChu 30013, Taiwan. E-mail: wkhsu@mx.nthu.edu.tw; Fax: 886-3-5722366; Tel: 886-3-5715131-35399

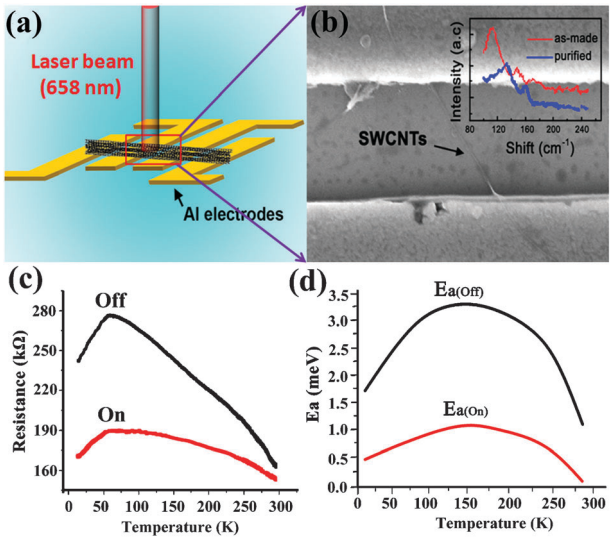

Fig. 1 (a) The device built for photocurrent generation. (b) An SEM image across a bundle of Al-electrodes, and the Raman spectrum (insert). (c) Resistance *vs.* temperature at beam-off (upper) and -on states (lower). (d) The E_a profiles at beam-off (upper) and -on states (lower).

We have fit Fig. 1c with power law and found $T^{0.23}$ below 60 K, excluding the Luttinger mechanism induced resistivity change ($T^{0.46}$).[11] For four-probe resistance measurements, the electric field essentially localizes at tube–lead contacts and the current magnitude only changes as the electrical potential drops over parallel conductive paths. Accordingly, the illumination induced resistance decrease here truly originates from optical effects, including photocurrent creation and bolometric heating. The latter, however, is unlikely, since photoexcitation induced resistance decrease normally exceeds that of a thermally-activated mechanism by one order of magnitude.[12] For example, the specific resistance (R/R_{RT}) at 150–300 K is 0.11–0.22 for the former and 0.01–0.07 for the latter. In other words, the results in Fig. 1c truly arise from optically excited semiconducting tubes in a bundle; this is further supported by micro-Raman data. We disperse SWCNTs onto a glass substrate, and several tiny aggregates visible through an optical microscope are excited with 2.41 eV wavelength. (1–5 μm, ×1000). The G-band (E_{2g}) appears to fit well with the Lorentzian model at 1550–1590 cm^{-1}, whereas the Breit–Wigner–Fano lineshape is barely seen, indicative of semiconducting tube dominated samples.[13] For a radial breathing mode (V_{RBM}) known as in-phase atomic vibration along the radial direction, the resonance frequency is detected at 138 and 160 cm^{-1} (insert, Fig. 1b), and the insertion of observed frequencies into the equation $V_{RBM} = 2320\ D^{-1}$ gives D = 1.46 nm and 1.68 nm, corresponding to (12, 10) and (16, 8) semiconducting tubes based on a Kataura plot.[14,15] In fact, the semiconductor tubes are expected in current devices since 2/3 of CNTs have been predicted to be non-metallic.[16] The question remains however as to why the CNT-device exhibits a crossover from negative to positive $d\rho/dT$ at 60 K. A similar transition has been observed in electron irradiated CNT bundles, and the underlying mechanism was believed to arise from conduction path diversion from radiatively damaged to undamaged tubes (*i.e.* from high to low resistive nanotubes).[17] In our study, illumination created lattice damage can be excluded, because the crossover also appears in the beam-off state, and repeat experiments yield a similar result. For CNT bundles, the electrical transport is dominated by inter-tube hopping, and the hopping probability (***P***) lies on 0.04–0.06 based on $E_a \sim$ 200–250 meV.[8] We have evaluated the ***P*** according to Mott's equation $\boldsymbol{P} \sim \exp[-2\alpha\boldsymbol{R}-E_a/k_BT]$ where α^{-1} is the attenuation length for a hydrogen-like localized wave function (5.9–7.1 nm) and the ***R*** is the spatial distance between localized states (1.54×10^6 cm^{-1} at $E_F = 7.55 \times 10^{19}$ eV^{-1} cm^{-3}).[7] For a tube bundle, the E_a corresponds to an intertube barrier and can be obtained by fitting Fig. 1c with a linear plot $\ln R = E_a/k_BT + A$, where A is the distance between the origin and intercepted points at the y-axis (Fig. 1d). At beam-off, the E_a is 1.25 meV at RT and increases to 3.25 meV at 100 K; the corresponding ***P*** being 0.21–0.33. Upon illumination, the E_a drops below 1 meV, whereas ***P*** increases to 0.35–0.5, implying a considerable leakage of photocarriers through the intertube hopping mechanism. Below 100 K, the E_a is reduced by 1.5 meV at dark and by 0.5 meV at bright states and the ***P*** decreases to 0.15–0.2 and 0.1–0.14, respectively (Fig. 1d). Here, we believe that the switching of the conduction path from semiconducting to metallic SWCNTs underlies the transition at 60 K. First, the resistivity of semiconducting tubes increases with decreasing temperature, so primary transport is expected at metallic tubes upon cooling, consistent with crossover in the E_a profile. Second, the positive $d\rho/dT$ at <60 K verifies the carrier conduction through optically inactive metallic nanotubes. Third, the ***P*** is significantly reduced below 60 K, supporting the carrier transport through individual metallic tubes. Fourth, the E_a begins to decrease below 100 K, facilitating transverse hopping of photo-carriers.[18,19]

Transverse conduction also implies nonradiative relaxation through intertube mechanisms, and is supported by Fig. 2a. The profiles show time-evolved resistance changes at 4 K, 60 K and RT, and the illumination interval is set at 20 s. At 4 K, the resistance decrease is 25%, and it reaches 46% at 60 K. The resistance decrease is small at RT (10%), and the relaxation induced tailing is attributable to inter-band thermalization. First, relaxation is not seen at 4 K and 60 K, second, the electron-hole recombination at elevated temperatures is a phonon assisted process,[4] and third, defect–trap states in CNTs are a thermally activated type.[5] The second and third points mentioned above also account for the low photocurrent creation at RT. We have evaluated the η according to equation below

$$\eta = \left[\frac{I_{photo}/q}{P_{inc}/h\upsilon}\right] \times 100\% \qquad (1)$$

where P_{inc} is the incident light power (= 1 mW) and I_{photo} is the short-circuit photocurrent extracted from Fig. 2a. The calculation then gives $\eta = 9 \times 10^{-3}$ at RT and 7.59×10^{-2} at 60 K; lower than that of isolated tubes by 1–2 orders of magnitude.[6] The η again decreases below 60 K and reaches 2.3×10^{-2} at 4 K; a value which is lower by threefold relative to the value detected at 60 K. The changeover from $\eta(T) \propto T^{-1}$ to $\eta(T) \propto T$ at 60 K is consistent with Fig. 1c and indicates different decay mechanisms of W_r. Fig. 2b plots I_{photo} *vs.* P_{inc} at different temperatures, and $I_{photo} \propto P_{inc}$ is obvious at 4 K

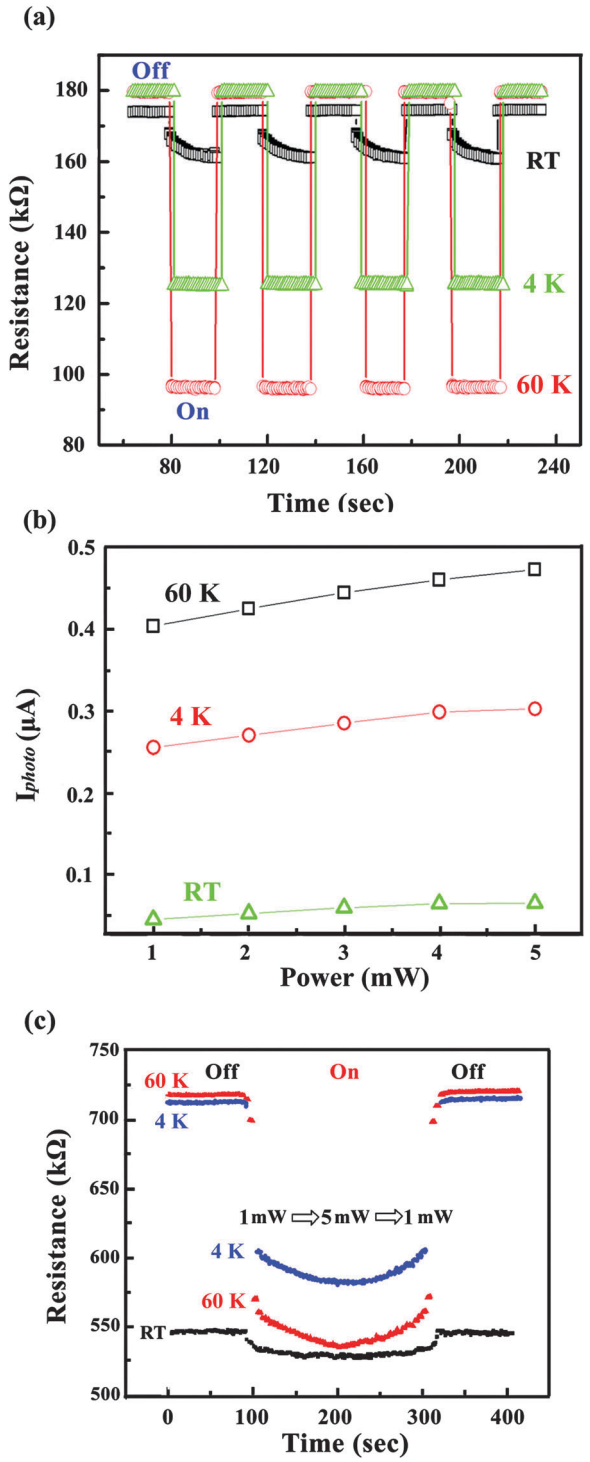

Fig. 2 (a) The time evolved resistance change at RT, 60 K and 4 K. (b) The I_{photo} *vs.* laser power at RT, 60 K and 4 K. (c) The time-evolved resistance change at 1 and 5 mW laser powers for a different sample.

and 60 K. The I_{photo} drops below 0.1 μA at RT and $I_{photo} \propto P_{inc}$ becomes insignificant, attributable to intertube mechanism induced photocarrier leakage.[20] First, the E_a is very small at the beam-on state (Fig. 1d), facilitating intertube hopping. Second, the photocurrent leakage means carrier deficiency at leads, consistent with low I_{photo}. In fact, the carrier deficiency also appears at 4–60 K and is evident by η decreasing with increasing P_{inc}, *i.e.* 7.5×10^{-2} (1 mW) → 2.8×10^{-2} (3 mW) → 1.7×10^{-2} (5 mW) at 60 K and 4.3×10^{-2} (1 mW) → 1.6×10^{-2} (3 mW) → 0.4×10^{-2} (5 mW) at 4 K. We have estimated the overall I_{photo} increase due to enhanced P_{inc} (1 mW → 5 mW), and found only 6–15% at 5 mW, relative to the initial value at 1 mW, again supporting a low η and photocurrent leakage. Compared with an isolated SWCNT the η and I_{photo} obtained at 60 K are still very low and a similar result is also detected in a different device containing 20–25 SWCNTs (Fig. 2c); the I_{photo} increase due to enhanced P_{inc} being 14% at 60 K ($\eta_{60\ K} = 6.8 \times 10^{-2}$), 9% at 4 K ($\eta_{4\ K} = 2.1 \times 10^{-2}$) and 4% at RT ($\eta_{RT} = 8.9 \times 10^{-3}$).

So far, the relationship of η with $\boldsymbol{P}$ and E_a has not been reported, and here we find $\boldsymbol{P} \propto \eta^{-1}$ and $E_a \propto \eta$ according to the analyses above. The question remains however as to why E_a is low in our nanotube bundles. The carrier transfer across intertube barriers has been well described using energy and momentum conservations, and junction resistance is reduced only when the Fermi wave vector between adjacent tubes aligns.[8] The conductivity of nanotube bundles has been improved by cation intercalation, and sandwiched charges were found to be acting as low barrier intertube channels.[21] Our elemental mapping (energy count, 50 000 ± 2%) carried out on purified SWCNTs shows a very low metal content (Fe < 0.01 wt%), and the capacitive reactance due to intercalated Fe particles between tubes is less than 0.1 Ω, excluding a sandwiched tube/Fe/tube structure. Here we believe that photocarriers leak through oxygenated lattices acting as low barrier channels, as supported by IR. For pristine SWCNTs the stretching modes of carboxy (C═O) and hydroxyl (C–OH) are detected at 1650 cm^{-1} and 1110 cm^{-1}, and the peak at 1400 cm^{-1} arises from the C–H bending mode (lower, Fig. 3a).[22,23] Similar spectra are also present in MWCNTs made by catalytic pyrolysis of acetylene, where the band intensity is greater by twofold, which is attributed to the increased material density.[9] The existing oxygenated groups in as-made CNTs have been previously discussed, and the oxygen was believed to originate from the precursors and alumina furnaces.[9] We find that oxygenated groups remain bound to CNT lattices after purification, and a blue-shift is absent (upper Fig. 3a), ruling out tube cutting induced dimerization of hydroxyl groups at open edges.[18] Additional evidence in supporting the absence of tube cutting comes from SEM inspections over 50 SWCNTs, and the distribution is found to peak at 1.8 μm, *ca.* 2–4% lower than that of the raw material (insert, Fig. 3a). We have estimated the O/C ratio based on Beer's law and integration of the band area.[9] Calculation gives 0.0024, corresponding to 400 carbon atoms (or 3.5–4 nm^{-1}) per oxygenated group. In practice, SWCNTs are aligned between electrodes, so the intertube channel (H_{inter}) can be evaluated by equation $H_{inter} = NL/D$ where N is the SWCNT quantity (= 10–15), L is the nanotube length (= 1.8 μm) and D is the density of the oxygenated group (= 3.5–4 nm^{-1}). Calculation yields H_{inter} = 6000–9000, accounting for the low I_{photo} detected here. Fig. 3b plots resistance against excitation wavelength at 60 K (triangles) and the η has been evaluated to be $0.9–2.1 \times 10^{-2}$, approximating the value observed in a different sample (squares). According to the photoselective resonance

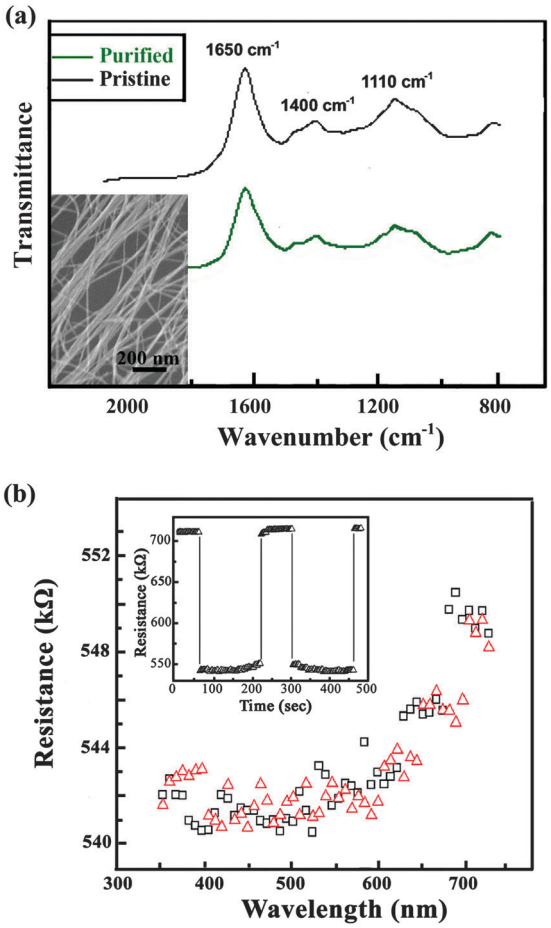

Fig. 3 (a) FTIR spectra of pristine (lower), and purified SWCNTs (upper), and an SEM image of purified SWCNTs supported on a TEM grid (insert). (b) Enlarged resistance *vs.* excitation wavelength profiles and original plots (insert).

rule, the optical transition in our samples should take place at 550–900 nm, and the absorption energy lies between 0.8–1.4 eV.[1,2] In Fig. 3b however, the resistance drops at a shorter wavelength (350 nm) and the corresponding absorption energy is 3.5 eV, implying a breaking of the CNT electronic symmetry by oxygenation created localized states. This outcome again supports the analyses above.

Yoon *et al.* have studied the conductance of crisscrossed SWCNTs upon compression, and found preferential tunneling of electrons at deformed lattices.[21] Conductance then drops by two orders of magnitude as the load is moved and the underlying mechanism is due to the $\check{\boldsymbol{R}}$ increase. We have calculated the density of states (DOS) based on the *ab initio* method and the procedure is as follows. Two zigzag tubes (5,0) consisting of 200 atoms are built within a 5 × 5 nm window and the centre-to-centre intertube separation is set at 5 Å. An oxygen atom is incorporated into the hexagonal lattice to form an epoxide and the C–O–C induced strain is limited within a hexagonal ring, similar to reported data.[21] The density function theory is treated with exchange–correlation and Perdew-Ultrasoft pseudo-potential, and the self-consistent field (SCF) tolerance threshold is set at 10^{-6} eV per atom for structure convergence and 0.04 $Å^{-1}$ for the Monkhorst–Pack k-point grid separation. DOS is calculated by the Gaussian-like smearing to eliminate discontinuous changes in energy band at E_F, and the mixing scheme of Pulay and the residual minimization in iterative subspace method is used for a faster convergence. The cut-off energy is set below 330 eV and band structure is simulated using standard k-point paths. Fig. 4a shows two tubes stacking in a crisscross fashion, and no commensurate alignment of electron wave vector is present at E_F; the band gap (E_g) and nonbonding energy between tubes being 0.7 eV and 2293 kJ mol^{-1}. In this case, carriers can only tunnel through σ* and π* states, and intertube hopping sites locate at the nearest lattices between tubes, equivalent to a coronene (yellow) (Fig. 4a). The oxygenation creates a metallic-like state near to the E_F, and E_g is reduced to 0.02 eV (Fig. 4b), supporting the photocurrent leakage through intertube hopping. First, the C–O dipole induces a radial deformation (Fig. 4b, top) and reduces $\check{\boldsymbol{R}}$ between tubes accordingly. Second, the created dipole state, which lies at a lower energy than that of the π* channel provides an extra intertube channel. Fig. 5 describes how I_{photo} is dissipated at present devices and aligned CNTs are considered as resistors connected in parallel

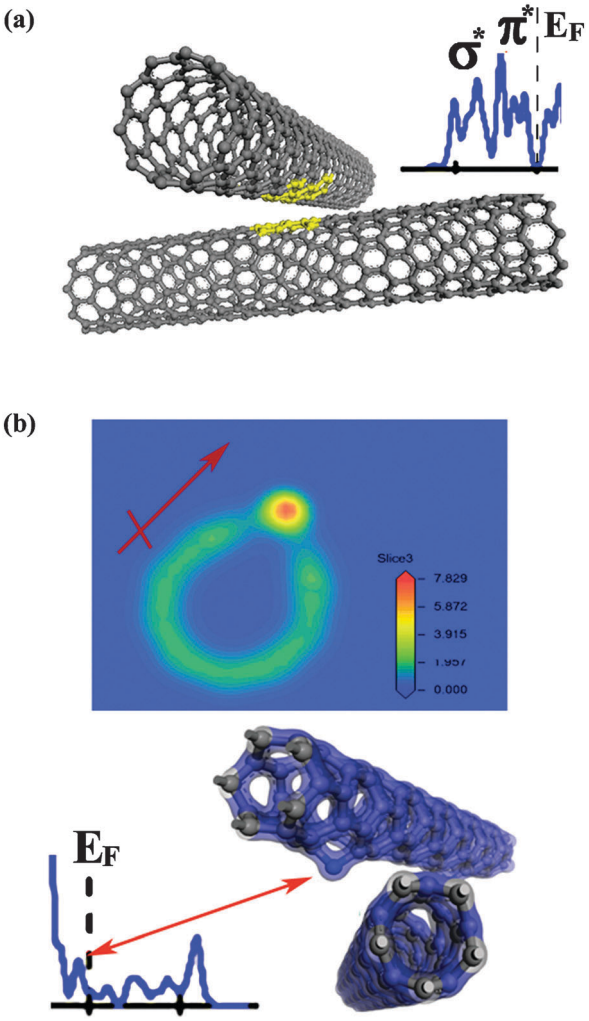

Fig. 4 (a) Simulated (5,0) tubes stacking in a crisscross fashion and corresponding DOS spectra (insert). (b) The charge distribution profile (top) and corresponding DOS spectra (lower).

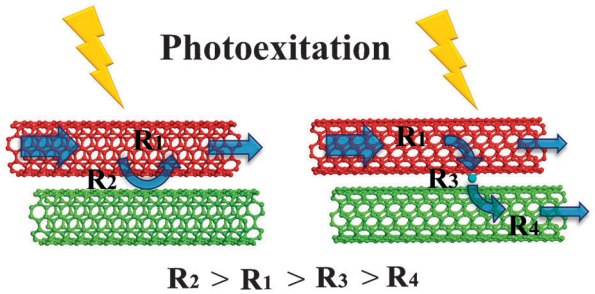

Fig. 5 The I_{photo} dissipation in pristine (left) and oxygenated tube bundles (right).

($\Sigma 1/R_n$, $n = 4$). The R_1 and R_4 represent electrical resistances of semiconducting and metallic tubes and, the R_2 and R_3 denote intertube barriers without and with epoxide bound to lattices; the resistance sequence being $R_2 > R_1 > R_3 > R_4$ according to Fig. 1c–d. Upon photoexcitation, the I_{photo} (Fig. 4b, arrow) is transported by semiconducting tubes (top) and dissipated by R_1 only (Fig. 4b, left panel). For oxygenated CNTs (Fig. 4b, right), the photocarriers due to $R_1 > R_3$ can travel in both longitudinal and transverse directions so optical gain is reduced by $R_1 + R_2 + R_3 + R_4$, accounting for low η and I_{photo}.

Conclusions

The diversion of the conduction path from semiconducting to metallic CNTs underlies the $d\rho/dT$ transition at 60 K, and the low I_{photo} is found to be related to photocarrier leakage through oxygenated lattices acting as low barrier channels between tubes. The H_{inter} in current devices has been estimated to be 6000–9000, and the corresponding $\boldsymbol{P}$ is 0.3–0.5.

Acknowledgements

We thank the National Science Council of Taiwan for the financial support (NSC-99-2112-M-007-014-MY2).

Notes and references

1 V. V. Deshpande, B. Chandra, R. Caldwell, D. S. Novikov, J. Hone and M. Bockrath, *Science*, 2009, **323**, 106.
2 S. M. Bachilo, M. S. Strano, C. Kittrell, R. H. Hauge, R. E. Smalley and R. B. Weisman, *Science*, 2002, **298**, 2361.
3 D. Karaiskaj, C. Engtrakkul, T. McDonald, M. J. Heben and A. Mascarenhas, *Phys. Rev. Lett.*, 2006, **96**, 106805-1.
4 W. K. Metzger, T. J. McDonald, C. Engtrakul, J. L. Blackburn, G. D. Scholes, G. Rumbles and M. J. Heben, *J. Phys. Chem. C*, 2007, **111**, 3601.
5 A. Hagen, M. Steiner, M. B. Raschke, C. Lienau, T. Hertel and H. Qian, *Phys. Rev. Lett.*, 2005, **95**, 197401-1.
6 S. Berger, C. Voisin, G. Cassabois, C. Delalande and P. Roussignol, *Nano Lett.*, 2007, **7**, 398.
7 M. Aggarwal, S. Khan, M. Husain, T. C. Ming, M. Y. Tsai, T. P. Perng and Z. H. Khan, *Eur. Phys. J. B*, 2007, **60**, 319.
8 M. S. Fuhrer, J. Nygård, L. Shih, M. Forero, Y.-G. Yoon, M. S. C. Mazzoni, H.-J. Choi, J. Ihm, S. G. Louie, A. Zettl and P. L. McEuen, *Science*, 2000, **288**, 494.
9 Y.-F. Li, C.-I. Hung, C.-C. Li, W. Chin, B.-Y. Wei and W.-K. Hsu, *J. Mater. Chem.*, 2009, **19**, 6761.
10 S.-H. Jhi, S. G. Louie and M. L. Cohen, *Phys. Rev. Lett.*, 2000, **85**, 1710.
11 M. Bockrath, D. H. Cobden, J. Lu, A. G. Rinzler, R. E. Smalley, J. Balents and P. L. McEuen, *Nature*, 1999, **397**, 598.
12 M. E. Itkis, E. Borondics, A.-P. Yu and R. C. Haddon, *Science*, 2006, **312**, 413.
13 M. S. Dresselhaus, G. Dresselhaus, R. Saito and A. Jorio, *Phys. Rep.*, 2005, **409**, 47.
14 P. C. Eklund, J. M. Holden and R. A. Jishi, *Carbon*, 1995, **33**, 959.
15 K. Kuzmany, B. Burger, A. Thess and R. E. Smalley, *Carbon*, 1998, **36**, 709.
16 H. Stahl, J. Appenzeller, R. Martel, Ph. Avouris and B. Lengeler, *Phys. Rev. Lett.*, 2000, **85**, 5186.
17 H.-C. Li, S.-Y. Lu, S.-H. Syue, W.-K. Hsu and S.-C. Chang, *Appl. Phys. Lett.*, 2008, **93**, 033104.
18 J. Hone, I. Ellwood, M. Muno, A. Mizel, M. L. Cohen and A. Zettl, *Phys. Rev. Lett.*, 1998, **80**, 1042.
19 A. Fujiwara, Y. Matsuoka, H. Suematsu, N. Ogawa, K. Miyano, H. Kataura, Y. Maniwa, S. Suzuki and Y. Achiba, *Carbon*, 2004, **42**, 919.
20 J.-L. Li, K. N. Kudin, M. J. McAllister, R. K. Prud'homme, I. A. Aksay and R. Car, *Phys. Rev. Lett.*, 2006, **96**, 176101.
21 Y. G. Yoon, M. S. C. Mazzoni, H. J. Choi, J. Ihm and S. G. Louie, *Phys. Rev. Lett.*, 2001, **86**, 688.
22 G.-X. Sun, G.-M. Chen, J. Liu, J.-P. Yang, J.-Y. Xie, Z.-P. Liu, R. Li and X. Li, *Polymer*, 2009, **50**, 5787.
23 C.-P. Yuan, J.-H. Zhang, G.-M. Chen and J.-P. Yang, *Chem. Commun.*, 2011, **47**, 899.